AIAA JOURNAL
Vol. 38, No. 8, August 2000

Parallel Computations of High-Lift Airfoil Flows Using Two-Equation Turbulence Models

Chang Sung Kim,* Chongam Kim,† and Oh Hyun Rho‡
Seoul National University, Seoul 151-742, Republic of Korea

Viscous turbulent flows over high-lift airfoils are investigated by using unsteady, incompressible, and compressible Reynolds-averaged Navier–Stokes equations under a parallel computing environment. Compressibility effects can be significant in the leading-edge region of high-lift airfoils with a highly loaded element. Thus, both the incompressible and compressible computations are performed to study the compressibility effects. The compressible code involves an upwind-differenced scheme for the convective terms and a lower–upper symmetric Gauss–Seidel scheme for temporal integration. The incompressible code with a pseudocompressibility method also adopts the same schemes as the compressible code. Both codes are parallel processed by using message passing interface programming method and show good parallel speedups. Three two-equation turbulence models (the standard k–ε, the k–ω, and the k–ω shear stress transport model) are carefully evaluated by computing the flows over single-element and multielement airfoils. The compressible and incompressible codes are validated by predicting the flow around the RAE 2822 transonic airfoil and NACA 4412 airfoil, respectively. In addition, both the incompressible and compressible codes using the Chimera overlapping grid scheme are used to compute the flow over the NLR 7301 airfoil with flap and the NASA GAW-1 high-lift airfoil. Compressibility effects on surface pressure coefficients, velocity profiles, and skin friction coefficients are numerically simulated.

Introduction

WITH the recent advancement of computer capability, the computational design method using computational fluid dynamics becomes a new trend in multielement airfoil design. Accurate and efficient calculations of the flow around a multielement airfoil are required to precede the practical design process. Thus, the interest of this work is focused on the incompressible and compressible computations of the viscous turbulent flow over high-lift airfoils under a parallel computing environment. In general, the flow over high-lift airfoils can be assumed to be incompressible because the freestream Mach number is approximately 0.1–0.4 and chord Reynolds numbers are usually 1×10^6 to 40×10^6 (Ref. 1). Thus, a parallelized incompressible Navier–Stokes code with a Chimera grid is developed for efficient computations. An incompressible code has the advantage over a compressible one of requiring less computation time, because the equation of energy transport is generally decoupled in the incompressible formulation, and compressible codes may have a slow convergence at these low freestream Mach numbers.[2] In fact, an incompressible code has been applied numerously to multielement airfoil design.[3–5] However, it may not be computationally cheaper to use an incompressible code over a compressible one to study poststall, unsteady airfoil flows. Furthermore, compressibility effects can be significant in some cases of multielement airfoils with highly loaded elements near the leading edge. For this reason, a parallelized compressible Navier–Stokes code with a Chimera grid is also developed, and its results are compared with those from the incompressible code. Both codes are parallel processed by using a message passing interface (MPI) programming method[6,7] on a Cray T3E parallel machine.

So far, many turbulence models, such as algebraic models, one-equation models, and two-equation models, have been developed for the engineering computations of various turbulent flows. It is, however, difficult to accurately predict viscous, turbulent flows around multielement airfoils, because of confluent boundary layers and massive flow separation at a high angle of attack near the stall angle. Unlike one- and two-equation models, algebraic models are inadequate for the flows over multielement airfoils because they require a delicate length scale. Many studies adopting one-equation models have been performed for the computations of such flows with a varying degree of success.[2,8,9] One-equation models may not be preferable for separated flows and wakes. Recently, two-equation turbulence models have been used for the turbulent flows over multielement airfoils.[9–11] In the present work, three two-equation turbulence models, the standard k–ε model,[12,13] the k–ω model of Wilcox,[12,14] and the k–ω shear stress transport (SST) model of Menter,[15,16] are carefully assessed through a computation of the flows over single-element and multielement airfoils. Several k–ε models involving different wall functions for the accurate calculation of the inner boundary layer have been developed and have shown good results. Unlike the k–ε models, the k–ω model does not need a wall function to resolve a viscous sublayer, which is quite suitable in parallel-processed programming. In contrast, the k–ε model is insensitive to the freestream turbulence level in the outer boundary layer, whereas the k–ω model is highly sensitive to freestream turbulence values.[14] Combining the advantages of the two models, the k–ω SST model is found to have the property of the original k–ω model in the near-wall region and of the k–ε model in the outer boundary layer.[15,16]

Both the compressible parallel code and incompressible parallel code with different two-equation turbulence models are examined by means of numerous computations. The compressible code is validated by computing the flow over the RAE 2822 transonic airfoil, and it shows a good property to predict surface pressure coefficients and velocity profiles in the boundary layers. The incompressible code is validated through computations of the flow over the NACA 4412 airfoil, for a wide range of angles of attack from zero to maximum lift. In particular, computations of the flow over the NLR 7301 airfoil with flap, and the NASA GAW-1 high-lift airfoil with a leading-edge slat and a trailing-edge flap, are performed by using both the incompressible and compressible code to study the compressibility effects on the flow near the high-loaded leading edge.

Numerical Background

Governing Equations

The governing equations are the two-dimensional, unsteady, compressible Navier–Stokes equations and are written in conservation law form as

Received 22 March 1999; revision received 12 September 1999; accepted for publication 12 December 1999.

*Graduate Research Assistant, Department of Aerospace Engineering. Student Member AIAA.

†Assistant Professor, Department of Aerospace Engineering. Member AIAA.

‡Professor, Department of Aerospace Engineering; aero@snu.ac.kr. Senior Member AIAA.

$$\frac{\partial \rho}{\partial t} + \frac{\partial}{\partial x_k}(\rho u_k) = 0$$

$$\frac{\partial}{\partial t}(\rho u_i) + \frac{\partial}{\partial x_j}(\rho u_i u_j) = -\frac{\partial p}{\partial x_i} + \frac{\partial \hat{\tau}_{ij}}{\partial x_j}$$

$$\frac{\partial \rho E}{\partial t} + \frac{\partial}{\partial x_j}(\rho E u_j) = -\frac{\partial p u_j}{\partial x_j} + \frac{\partial}{\partial x_j}[u_i \hat{\tau}_{ij} - q_j] \tag{1}$$

where E is the total energy and $\hat{\tau}_{ij}$ are the sum of molecular and Reynolds stresses defined as

$$\hat{\tau}_{ij} = 2\mu\left(S_{ij} - \frac{S_{kk}\delta_{ij}}{3}\right) + \tau_{ij}$$

$$\tau_{ij} = 2\mu_T\left(S_{ij} - \frac{S_{kk}\delta_{ij}}{3}\right) - \frac{2\rho k \delta_{ij}}{3}, \qquad S_{ij} = \frac{1}{2}\left(\frac{\partial u_i}{\partial x_j} + \frac{\partial u_j}{\partial x_i}\right)$$

and q_j is the total heat-flux rate defined as

$$q_j = -\left(\frac{\gamma}{\gamma - 1}\right)\left(\frac{\mu}{Pr} + \frac{\mu_T}{Pr_T}\right)\frac{\partial T}{\partial x_j}$$

The perfect gas equation of state is introduced to complete the set of compressible equations as

$$p = \rho(\gamma - 1)\left[E - \tfrac{1}{2}u_i u_i\right] \tag{2}$$

For incompressible problems, the energy equation does not have to be included unless heat transfer is a matter of concern.

Turbulence Models

In this work, the standard k–ε model[12,13] without wall functions, the k–ω model,[12,14] and the k–ω SST model[15,16] are evaluated to predict the viscous turbulent flows over high-lift airfoils. The k–ω SST model combining the k–ω model with the k–ε model is written as follows:

$$\frac{\partial \rho k}{\partial t} + \frac{\partial}{\partial x_j}(\rho k u_j) = \tau_{ij}\frac{\partial u_i}{\partial x_j} - \beta^* \rho \omega k + \frac{\partial}{\partial x_j}\left((\mu + \sigma_k \mu_T)\frac{\partial k}{\partial x_j}\right)$$

$$\frac{\partial \rho \omega}{\partial t} + \frac{\partial}{\partial x_j}(\rho \omega u_j) = \frac{\gamma}{\nu_T}\tau_{ij}\frac{\partial u_i}{\partial x_j} - \beta \rho \omega^2$$

$$+ \frac{\partial}{\partial x_j}\left((\mu + \sigma_\omega \mu_T)\frac{\partial \omega}{\partial x_j}\right) + 2(1 - F_1)\rho \sigma_{\omega_2}\frac{1}{\omega}\frac{\partial k}{\partial x_j}\frac{\partial \omega}{\partial x_j} \tag{3}$$

The combined constants are calculated in the following relation:

$$\Phi = F_1 \Phi_1 + (1 - F_1)\Phi_2$$

where Φ_1 represent the constants of the k–ω model except for σ_{k_1} and γ_1 (Refs. 13 and 14),

$$\sigma_{k_1} = 0.85, \qquad \sigma_{\omega_1} = 0.5, \qquad \beta_1 = 0.075, \qquad \beta^* = 0.09$$

$$\kappa = 0.41, \qquad \gamma_1 = \beta_1 \big|\, \beta^* - \sigma_{\omega_1}\kappa^2 \big|\, \sqrt{\beta^*}$$

and Φ_2 represent the constants of the k–ε model as[13]

$$\sigma_{k_2} = 1.0, \qquad \sigma_{\omega_2} = 0.856, \qquad \beta_2 = 0.0828, \qquad \beta^* = 0.09$$

$$\kappa = 0.41, \qquad \gamma_2 = \beta_2 \big|\, \beta^* - \sigma_{\omega_2}\kappa^2 \big|\, \sqrt{\beta^*}$$

Here F_1 is set to be zero for the k–ε model and one for the k–ω model. For the k–ω SST model, F_1 is defined as follows:

$$F_1 = \tanh\left[\left(\min\left\{\max\left(\frac{\sqrt{k}}{\beta^* \omega y}; \frac{500\nu}{y^2 \omega}\right); \frac{4\rho\sigma_{\omega_2}k}{\mathrm{CD}_{kw}\, y^2}\right\}\right)^4\right]$$

where y is the distance to the nearest surface and $\mathrm{CD}_{k\omega}$ is the positive portion of the cross-diffusion term:

$$\mathrm{CD}_{k\omega} = \max\left(2\rho\sigma_{\omega_2}\frac{1}{\omega}\frac{\partial k}{\partial x_j}\frac{\partial \omega}{\partial x_j}; 10^{-20}\right)$$

The eddy viscosity is defined to account for the transport of the principal turbulent shear stress as follows:

$$\mu_T = \rho k / \max(\omega; \Omega F_2 / 0.31)$$

where Ω is the absolute value of the vorticity and

$$F_2 = \tanh\left(\left\{\max\left(\frac{2\sqrt{k}}{\beta^* \omega y}; \frac{500\nu}{y^2 \omega}\right)\right\}^2\right)$$

Numerical Approach

The governing equations are discretized with a finite-volume method. For the compressible code, convective terms are upwind-differenced based on Roe's flux difference splitting (FDS) scheme.[17] A monotone upstream centered scheme for conservation laws approach[18] using a third-order interpolation is used to obtain a higher order of spatial accuracy. The third order of spatial accuracy is kept in all calculations. For a temporal integration, Yoon's lower–upper symmetric Gauss–Seidel scheme[19] is adopted. The incompressible code using the following pseudocompressibility relation has the same spatial and temporal schemes as the compressible code:

$$\frac{\partial p}{\partial \tau} = -\beta \nabla \cdot u \tag{4}$$

where τ denotes pseudotime and β is a pseudocompressibility parameter. Numerical experiments must be performed to determine a value of β yielding the best convergence.

Because a multielement airfoil generally has a complex geometry, it is very difficult to generate a high-quality grid system in a single block. Thus, patched grids, overlapping grids, or unstructured grids are popularly adopted. In this study, the overlapping grid approach known as the Chimera grid scheme[20] is used for an efficient grid generation. Subgrids around flap and slat are overlapped on the main grid around the basic airfoil. Information is exchanged between the subgrid and main grid domain through bilinear interpolation, which is found to be robust and easy to implement.

Wall boundary conditions are applied explicitly with no-slip condition. The pressure is extrapolated from the interior points and the other variables are specified from the freestream values at the inflow, whereas the pressure is specified and the other variables are extrapolated from the interior points at the outflow.

For the angles of attack near maximum lift, steady-state computations using a local time-stepping method do not converge completely. In these cases, unsteady computations must be performed in a time-accurate manner. Thus, the dual time-stepping method is adopted both in the incompressible and compressible codes.

Parallel-Processing Algorithm for the Chimera Grid

The search routines for fringe cells and donor cells are preprocessed. A fringe cell is to receive the flow information from four donor cells in an overlapped grid domain as shown in Fig. 1. A parallel process for the chimera grid (known as the PPCG algorithm, hereafter) is implemented as follows.

Step 1. Divide the main grid and subgrids into subdomains, considering load balance.

Step 2. Search each subdomain for fringe cells and donor cells.

Step 3. MPI_send and MPI_receive the flow information of donor cells from each processor to processor 0.

Step 4. Calculate the conservative variables of fringe cells through bilinear interpolation in processor 0.

Step 5. MPI_send and MPI_receive the flow information of fringe cells from processor 0 to each processor.

Step 6. Repeat the process from step 3 to step 5 until converged solutions are obtained.

The PPCG algorithm is found to be simple and efficient to implement in the parallel computations for the flows over multielement airfoils.

Results and Discussion

Both the compressible code and incompressible code were parallel processed by using the MPI programming method. The same grid

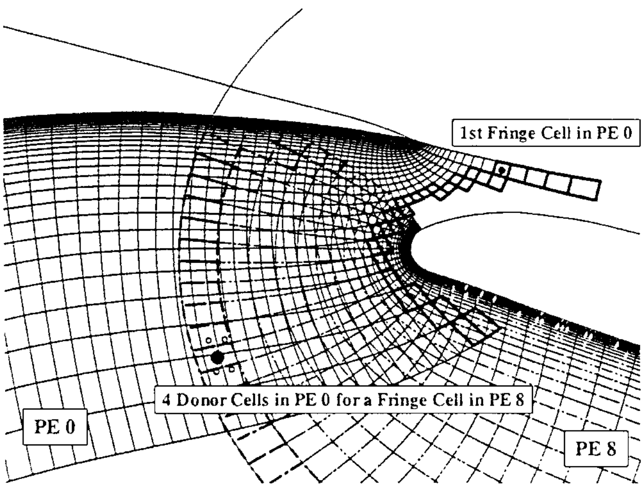

Fig. 1 Parallel implementation on a Chimera overlaid grid system; PE, processor element.

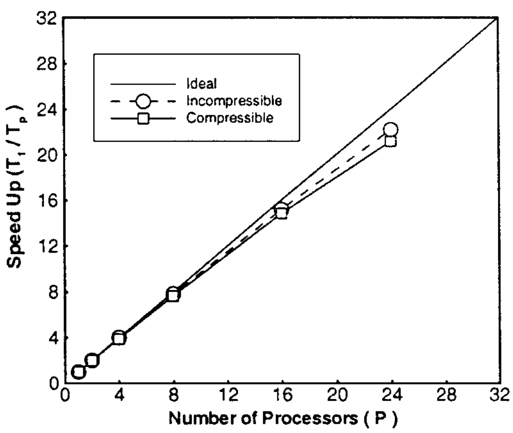

Fig. 2 Parallel speedup for single airfoil case using the incompressible and compressible codes.

points were distributed in all subdomains for load balance. Figure 2 shows the parallel speedup of the compressible and incompressible codes, using 1–24 processors. The parallel speedup was defined by the ratio of computing times according to the number of processors. Both codes show a good parallel speedup on the Cray T3E parallel machine.

RAE 2822 Transonic Airfoil

The flow over the RAE 2822 transonic airfoil with a maximum thickness of 12.1% of chord and a sharp trailing edge was computed to validate the compressible code at the Mach number of 0.73 and the Reynolds number of 6.5×10^6. A 129×65 hyperbolic O-grid was used with the spacing at the wall of 1×10^{-5} based on unit chord length. Also a 241×81 O-grid with the wall spacing of a 5×10^{-6} chord was used to test the sensitivity to grid resolution. The outer boundary was extended to 25 chords.

Computed results from the standard k–ε model, the k–ω model, and the k–ω SST model were compared with the experimental data presented by Cook et al.[21] at the angle of attack of 2.79 deg. Comparisons among computed and measured lift, drag, and pitching moment coefficients are shown in Table 1.

All the three turbulence models had little sensitivity to grid resolution in the sense that the computed results from the coarse and fine mesh were almost the same. Computed surface pressure coefficients using the fine mesh are compared with experimental data in Fig. 3. All models show a slight difference in shock wave position compared with the experimental data. The k–ω model shows a difference in shock wave position compared with the other two turbulence models. Figure 4 shows velocity profiles from the upper surface boundary layer at the stations of $x/c = 0.574$, 0.650, 0.750, and 0.900, using the fine mesh. The k–ω SST model yields a better agreement with experimental velocity profiles in the downstream region after the

Table 1 Comparison of computed and measured load coefficients[a]

Coefficient[b]	k–ε	k–ω	k–ω SST	Exp.
C_L	0.7957	0.8486	0.7910	0.803
$C_D(p)$	0.01299	0.01446	0.01228	——
$C_D(v)$	0.00733	0.00591	0.00519	——
C_D	0.02032	0.02037	0.01747	0.0168
C_M	−0.09406	−0.10518	−0.09245	−0.099

[a]RAE 2822, $M = 0.73$, $Re = 6.5 \times 10^6$, $\alpha = 2.79$ deg.
[b]$C_D(p)$, pressure drag; $C_D(v)$, skin friction drag.

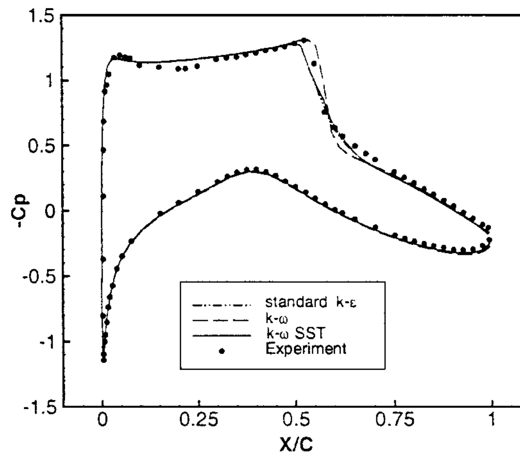

Fig. 3 Surface pressure coefficients over the RAE 2822 airfoil at α = 2.79 deg, M = 0.73, and Re = 6.5×10^6.

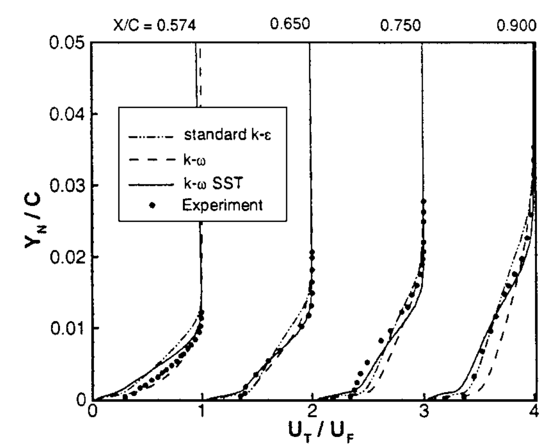

Fig. 4 Velocity profiles on the upper surface of the RAE 2822 airfoil at α = 2.79 deg.

shock wave, whereas the k–ω model produces a better performance in the immediate vicinity of the shock wave. The convergence histories of the compressible code using three turbulence models are shown in Fig. 5. The maximum iteration count was 10,000 and the maximum residual was less than 10^{-4} in ~2000 iterations. For the coarse mesh of 129×65 size, the computing time using 24 processors takes ~40 s for 2000 iterations on the Cray T3E parallel machine.

NACA 4412 Airfoil with Separation

The flow over the NACA 4412 airfoil was computed to validate the incompressible code at a Reynolds number of 1.52×10^6. A 245×65 hyperbolic O-grid was used with the wall spacing of a 1×10^{-5} chord and the outer boundary was extended to 25 chords.

Computed results from the standard k–ε model, the k–ω model, and k–ω SST model were compared with the experimental data presented by Coles and Wadcock[22] at the angle of attack of 13.87 deg for which a steady trailing-edge separation occurs. Trip-strips were employed in the experiment on the suction and pressure sides at $x/c = 0.025$ and 0.103, respectively. The production term in the transport equation for the turbulent kinetic energy was set to zero upstream of these locations to represent transition effects. Computed surface pressure coefficients with and without transition were

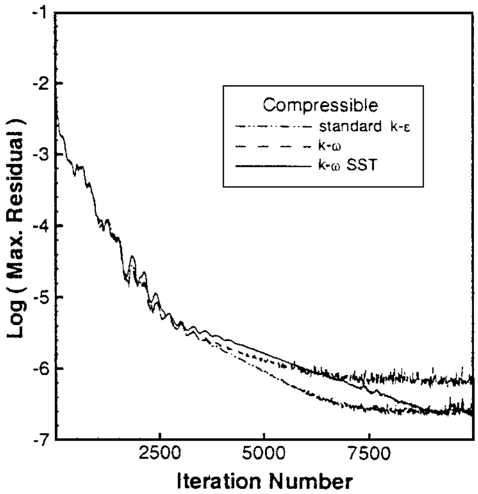

Fig. 5 Convergence history for the compressible flow over the RAE 2822 airfoil.

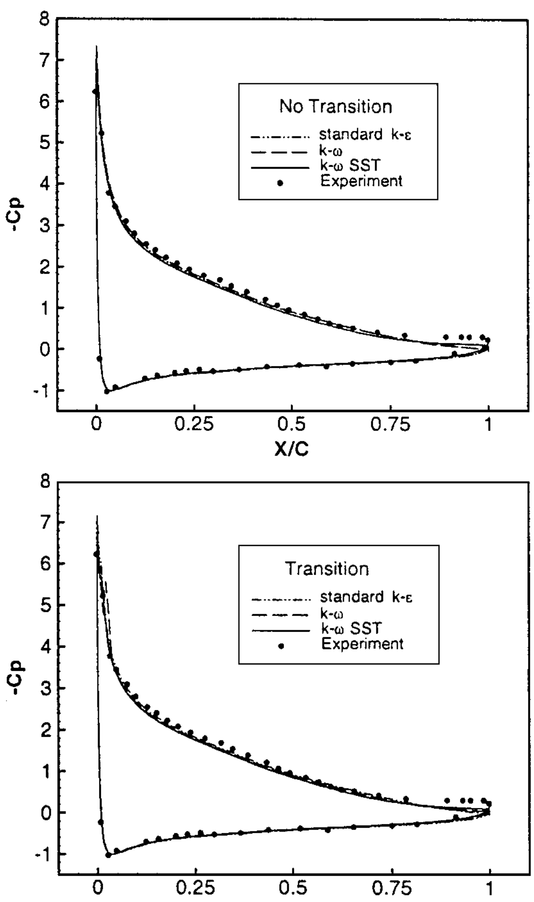

Fig. 6 Surface pressure coefficients over a NACA 4412 airfoil at α = 13.87 deg and *Re* = 1.52×10^6.

compared with experimental data in Fig. 6. Transition has a slight effect on the surface pressure coefficients from the k–ω SST model but has little effect on those from the standard k–ε or the k–ω model. The transition effect can be seen more clearly by comparing the velocity profiles from the upper surface boundary layer at the stations of x/c =0.620, 0.731, 0.842, and 0.897 in Fig. 7. The k–ω SST model shows a fairly good agreement with experimental velocity profiles in the downstream adverse pressure gradient region, whereas the standard k–ε model and the k–ω model yield quite a difference.

Convergence characteristics were sensitive to the value of β. It was found that the incompressible code converged well for the β of 20–200 through numerical tests. The convergence histories of the code for the three turbulence models are shown in Fig. 8. It can be

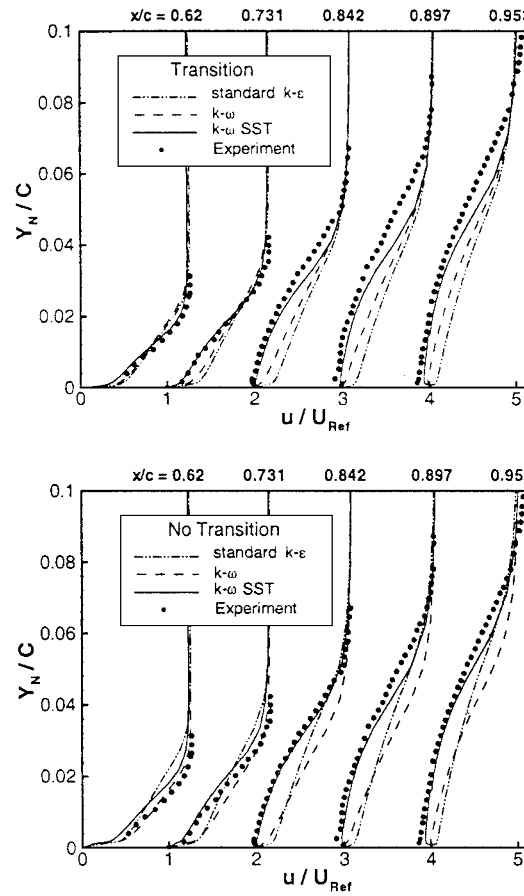

Fig. 7 Velocity profiles on the upper surface of a NACA 4412 airfoil at α = 13.87 deg.

seen that transitions slightly delay convergence characteristics. The maximum iteration count was 10,000, and the maximum residual of the continuity equation was less than 10^{-4} in ~3000 iterations. For the 245 × 65 mesh, computation time on the Cray T3E using 24 processors is ~72 s for 3000 iterations.

Figure 9 shows lift coefficients at the wide range of angles of attack from zero to maximum lift. The k–ω SST model with transition gives a closer agreement in the lift, especially in the prediction of stall. For the high angles of attack over 13.87 deg, steady-state computations overestimate the flow separation massively and do not converge completely. In these cases, unsteady computations with the dual time-stepping method were performed in a time-accurate manner. For 16 deg, lift coefficients vs time are shown in Fig. 10. Although the standard k–ε model converges to a steady-state solution, the k–ω model and the k–ω SST model show a periodic unsteadiness. For the k–ω and k–ω SST models with transition, the leading-edge laminar bubble is periodically shedding downstream to the trailing edge with different modes. Unsteady computations were performed with the nondimensional time step of 0.05 until the nondimensional time reached 800. For each physical time step, 30–40 subiterations were required until both the maximum divergence of velocity and the maximum residual were less than 10^{-4}.

Two-Element Airfoil

Compressible and incompressible computations for the flow over the NLR 7301 with a 32%c flap were performed at a Mach number of 0.185 and a Reynolds number of 2.51 ×10^6. The flap was positioned with a deflection angle of 20 deg, an overlap of 5.3%c, and a gap of 2.6%c in the experiment by Berg.[23] A 249 ×81 O-grid for the basic airfoil and a 125 ×41 O-grid for the flap was used for the Chimera grid scheme with the wall spacing of the order of a 10^{-6} chord. The outer boundary was extended to ~30 chords.

Figure 11 shows the parallel speedup of the incompressible and compressible codes adopting the PPCG algorithm, using 5–20 processors. Because the main grid had a grid size four times larger than that of the subgrid, the processors were distributed as evenly as

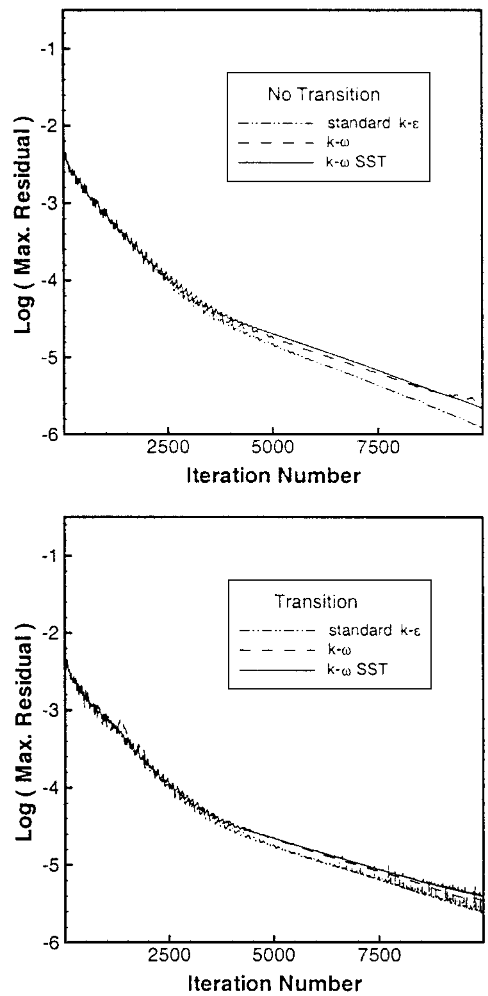

Fig. 8 Convergence history for the incompressible flow over a NACA 4412 airfoil.

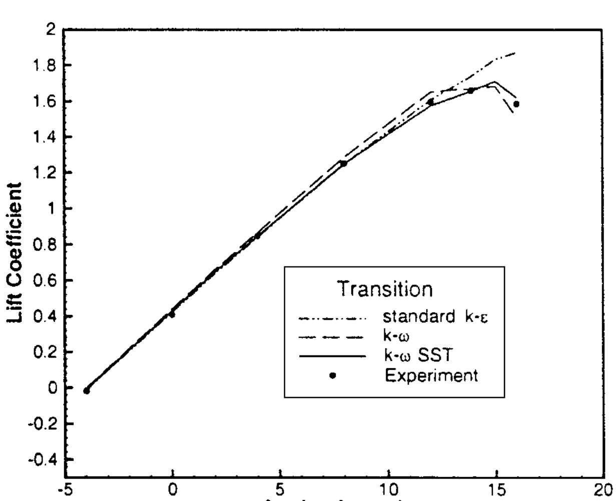

Fig. 9 Lift coefficient vs angle of attack for a NACA 4412 airfoil.

possible, proportional to the grid size for load balance. When five processors were used, four processors were given for the main grid and one processor for the subgrid. When 20 processors were used, 16 processors were given for the main grid and four processors for the subgrid. Both the incompressible and compressible codes show a good parallel speedup on the Cray T3E parallel machine.

Computed surface pressure coefficients are compared with the experimental data at an angle of attack of 6.0 deg in Fig. 12. The local peak Mach number near the leading edge is ~0.54 at this angle of attack. The incompressible and compressible results are similar, even in the suction peak at the leading edge of the basic airfoil. All

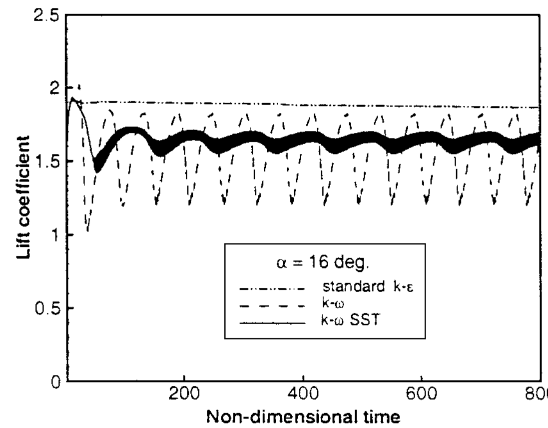

Fig. 10 Lift coefficient vs time for a NACA 4412 airfoil at α = 16 deg.

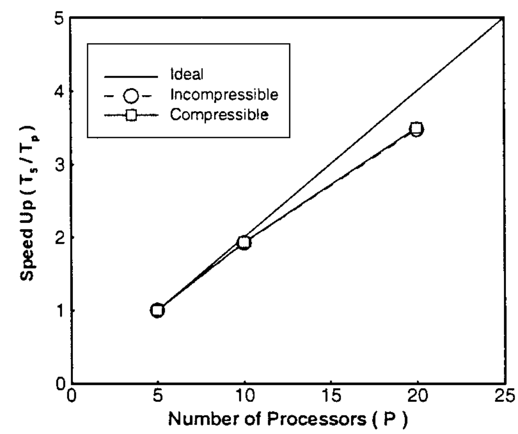

Fig. 11 Parallel speedup for the two-element airfoil case using a Chimera grid scheme.

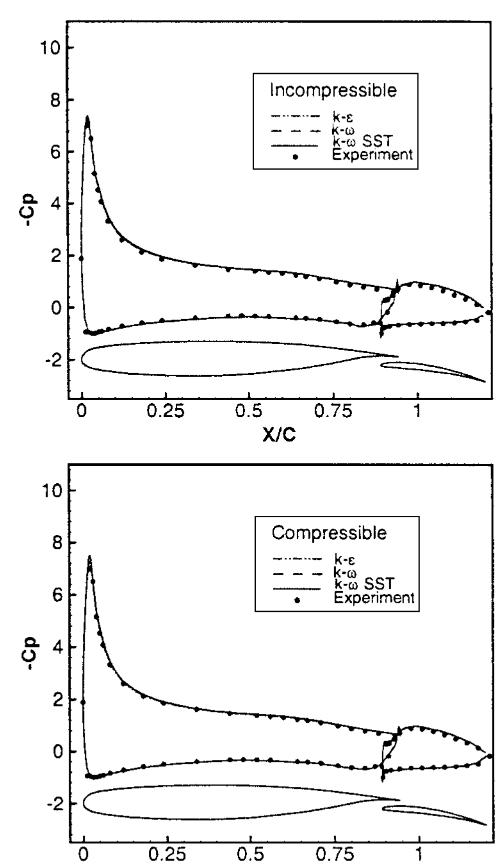

Fig. 12 Surface pressure coefficients over the NLR 7301 airfoil with flap at α = 6.0 deg, M = 0.185, and Re = 2.51×10^6.

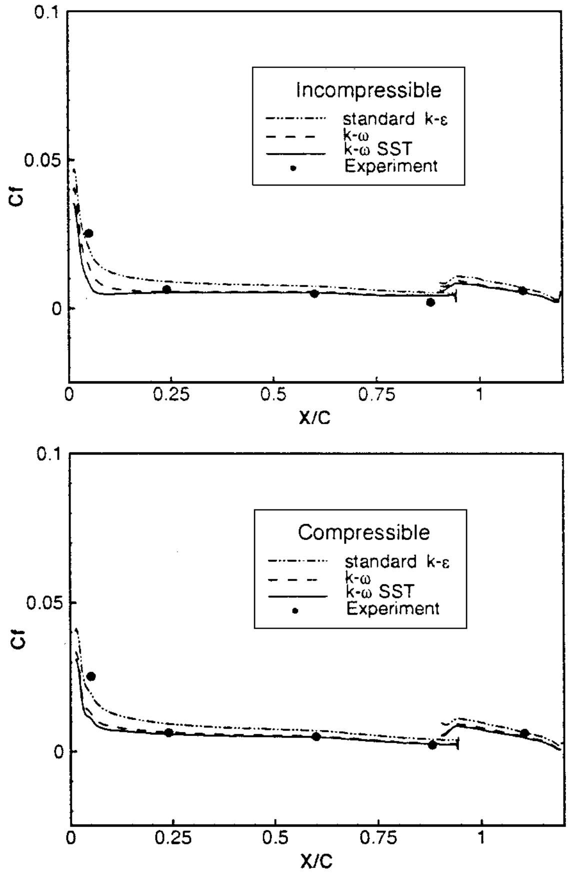

Fig. 13 Skin friction coefficients on the upper surface of the NLR 7301 airfoil with flap at α = 6.0 deg.

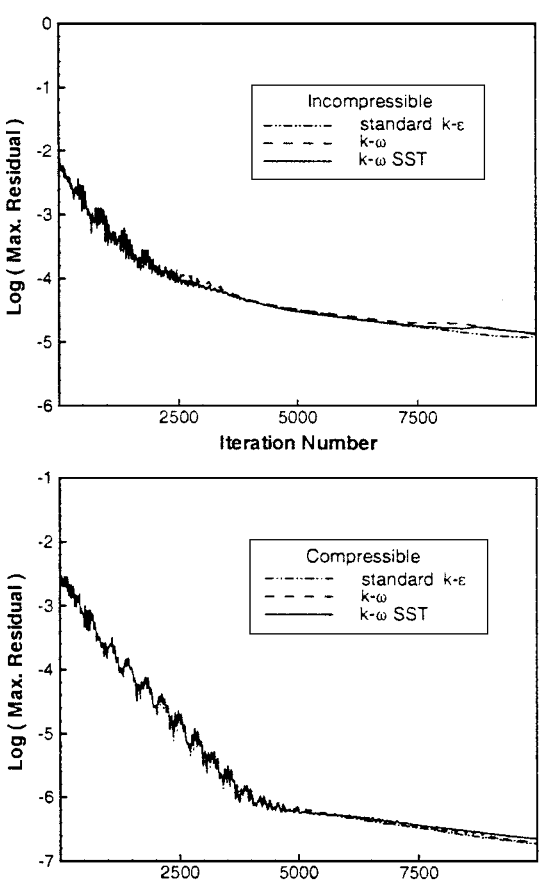

Fig. 14 Convergence history for the flow over the NLR 7301 airfoil with flap.

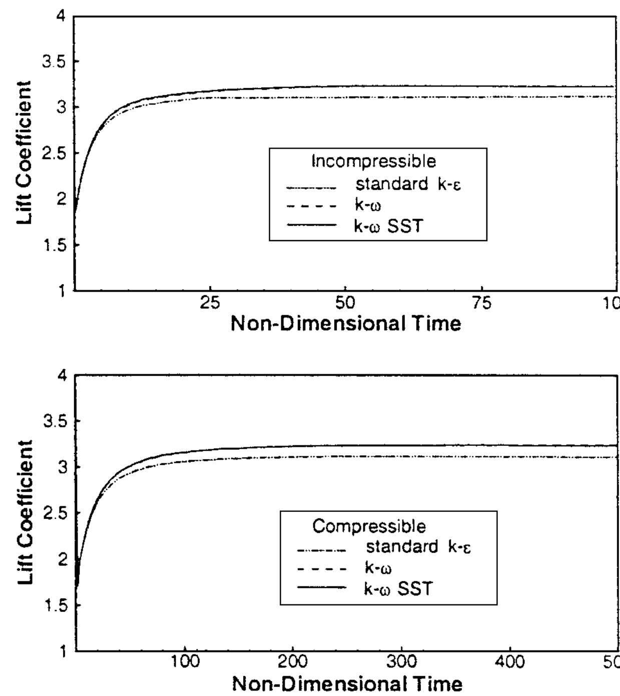

Fig. 15 Lift coefficient vs time for the NLR 7301 airfoil with flap at α = 13.1 deg in unsteady computations.

computations using the standard k–ε model, the k–ω model, and the k–ω SST model give a fairly good agreement with the experimental data. Computed skin friction coefficients are compared with the experimental data in Fig. 13. It is found that the flow is attached downstream to the trailing edge.

The convergence histories of the incompressible and compressible codes with three turbulence models are shown in Fig. 14. For the incompressible computations, the maximum iteration count was 10,000 and the maximum residual was less than 10^{-4} in ~3000 iterations. Computation time is ~160 s for 3000 iterations on the Cray T3E using 20 processors. For the compressible computations, converged solutions are obtained in ~3000 iterations. Computation time on the Cray T3E using 20 processors is ~240 s for 3000 iterations.

For the critical angle of attack of 13.1 deg where no flow separation is observed downstream to the trailing edge except for a very tiny laminar separation bubble near the leading edge in the experiment, both the steady-state incompressible and compressible computations predicted massive flow separation and did not converge completely. For this reason, computations were performed in a time-accurate, unsteady manner using the dual time-stepping method. Figure 15 shows lift coefficients vs time at this angle of attack. Incompressible computations were performed with the nondimensional time step of 0.01 and converged in 4000 physical time steps. The computation time using 20 processors was ~6100 s. Compressible computations were performed with the nondimensional time step of 0.1 and converged in 2000 physical time steps. The computation time using 20 processors was ~6900 s. In both cases, 5–40 subiterations were required for each time step during the course of the calculations. In the cases of time-accurate computations, it was found that the incompressible code had little advantage in terms of computation time over the compressible code.

Computed surface pressure coefficients are compared with the experimental data at 13.1 deg in Fig. 16. A discrepancy between the incompressible and compressible results is shown in the suction peak near the leading edge of the basic airfoil. For the freestream Mach number of 0.185, compressibility effects near the suction peak become significant because the local Mach number near the leading edge can be as large as 0.72. Figure 17 shows the velocity profiles at $x/c = 0.05, 0.94$ on the basic airfoil and at $x_F/c = 0.119, 0.219$ on the upper flap surface. The incompressible and compressible results are similar except at the 5% chord position. This is more evident by comparing the velocity profiles at the 5% chord position

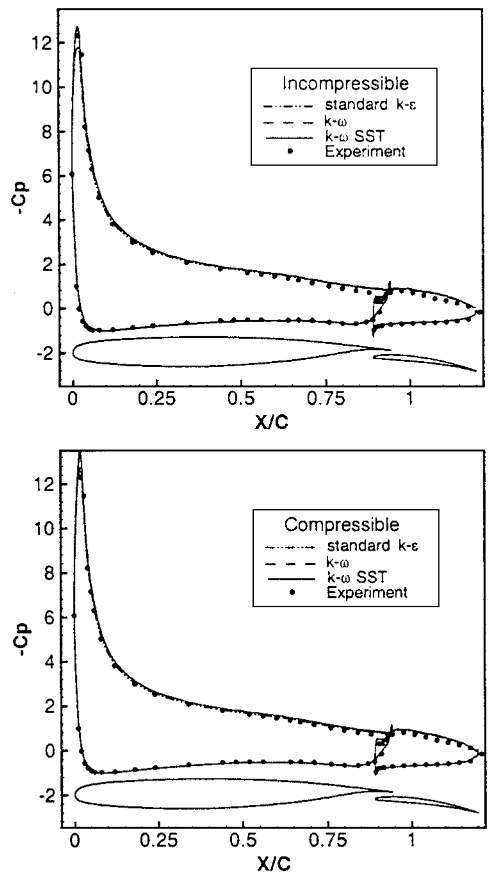

Fig. 16 Surface pressure coefficients over the NLR 7301 airfoil with flap at α = 13.1 deg by unsteady computations.

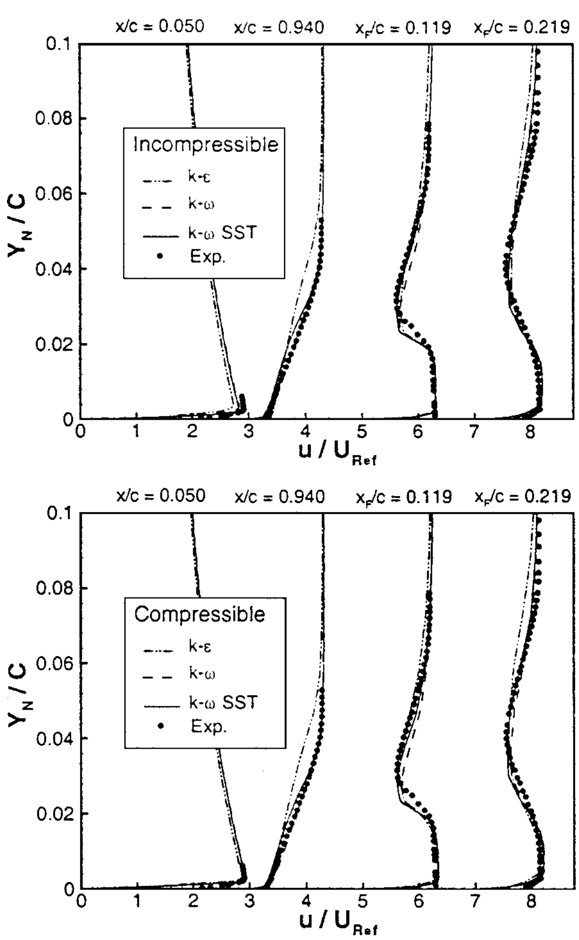

Fig. 17 Velocity profiles on the upper surfaces of the NLR 7301 airfoil with flap at α = 13.1 deg.

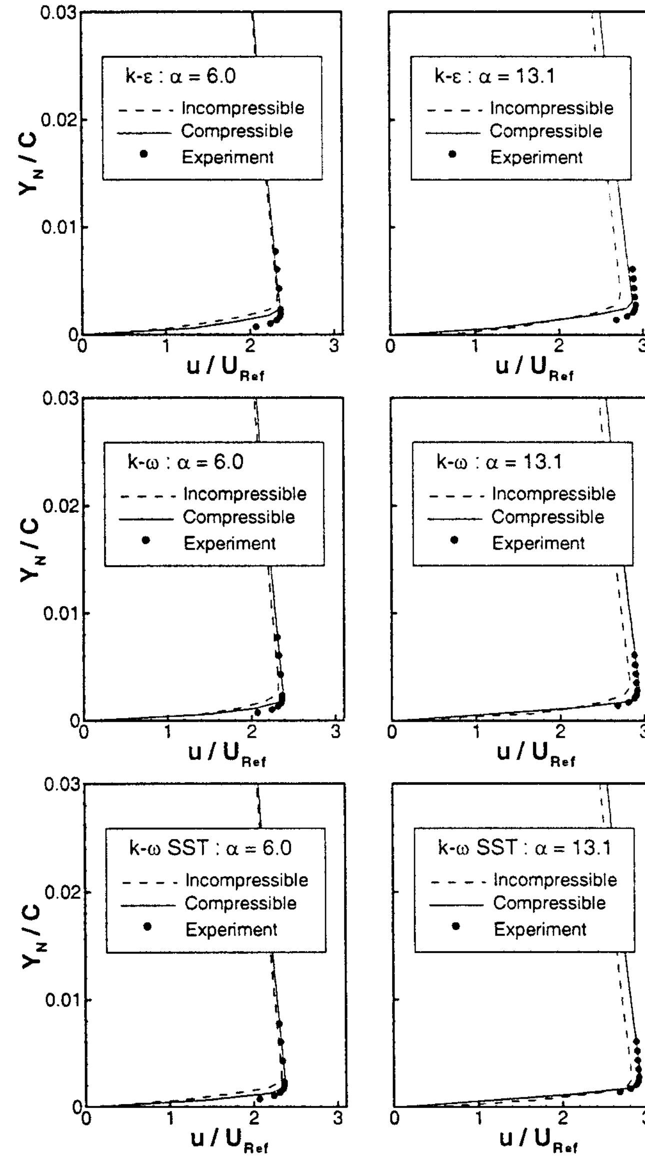

Fig. 18 Compressibility effects on velocity profiles at a 5% chord for the NLR 7301 airfoil with flap.

at the angles of attack of 6 and 13.1 deg shown in Fig. 18. The discrepancy between the incompressible and compressible velocity profiles is considerable at 13.1 deg. Compressibility effects can be significant as angle of attack increases even at the same freestream Mach number.

Three-Element Airfoil

Also as in the two-element airfoil case, both the parallelized incompressible and compressible codes were successfully implemented to computations for the flow over the 17%c thick NASA GAW-1 airfoil with a 15%c leading-edge slat and a 29%c trailing-edge flap. The slat was positioned with a deflection angle of 42 deg, an overlap of 1.5%c, and a gap of 1.5%c, whereas the flap was positioned with a deflection angle of 30 deg, an overlap of 0.0%c, and a gap of 2.5%c. The experiment was carried out at a Mach number of 0.15 and a Reynolds number of 0.62 $\times 10^6$ by Braden et al.[24] A 249 $\times$ 81 O-grid for the basic airfoil, a 125 $\times$ 41 O-grid for the slat, and a 125 $\times$ 41 O-grid for the flap were used for the Chimera grid scheme with the wall spacing of the order of a 10^{-5} chord. The outer boundary was extended to $\sim$30 chords.

Figure 19 shows the parallel speedup of the incompressible and compressible code using from 6 to 24 processors. Because the main grid had a grid size four times larger than that of the subgrids, the processors were distributed proportional to the grid size for load balance. For example, four processors were given for the main grid and one processor each was given for the slat and flap grids.

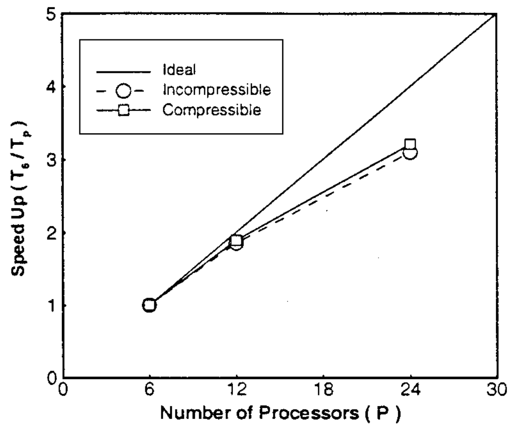

Fig. 19 Parallel speedup for the three-element airfoil case using a Chimera grid scheme.

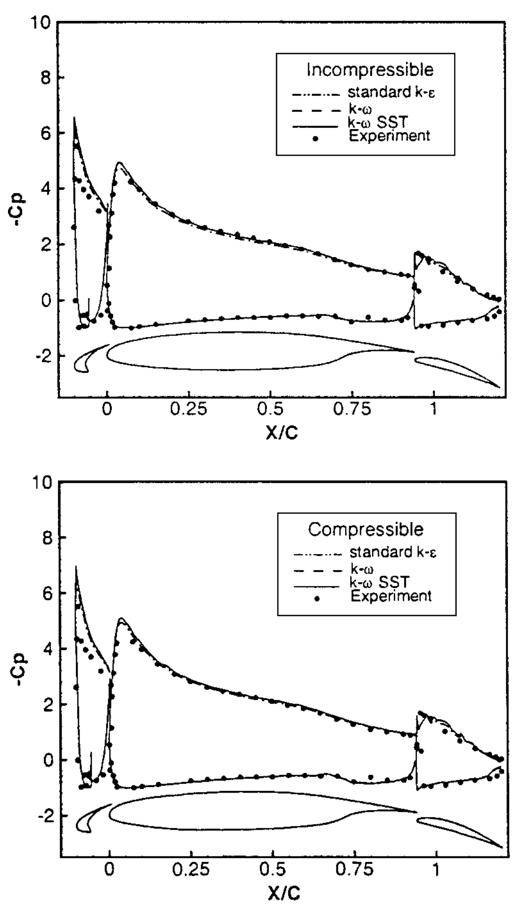

Fig. 20 Surface pressure coefficients over the GAW-1 high-lift airfoil at α = 12 deg, M = 0.15, and Re = 0.62×10^6.

Computed surface pressure coefficients are compared with the experimental data at an angle of attack of 12.0 deg in Fig. 20. For both incompressible and compressible computations, a discrepancy between the computational and experimental results is found on the suction surface of the slat and flap that is due to the ambiguity in flap and slat position. The three turbulence models give slight differences in surface pressure coefficients at this angle of attack. The convergence history of the three-element airfoil case is similar to that of the two-element airfoil case in Fig. 14. For the incompressible computations, the maximum iteration count was 10,000 and the maximum residual was less than 10^{-4} in ~3000 iterations. Computation time using 24 processors is ~180 s for 3000 iterations on the Cray T3E. For the compressible computations, converged solutions are obtained in ~3000 iterations. Computation time using 24 processors is ~290 s for 3000 iterations.

Conclusion

Both compressible and incompressible computations were performed for the viscous turbulent flows over high-lift airfoils by using two-equation turbulence models under a parallel computing environment. The parallelized compressible and incompressible flow solvers on a Chimera grid showed fairly good parallel speedups. The three turbulence models of the standard k–ε model, the k–ω model, and the k–ω SST model were evaluated by comparing the surface pressure coefficients, skin friction coefficients, and velocity profiles in the boundary layers with the experimental data. Overall, the k–ω SST model shows a better performance compared with the other two-equation models in predicting the adverse pressure gradient region on the suction surface of high-lift airfoils. In particular, the flow over the NLR 7301 airfoil with a flap was carefully investigated by using both the incompressible and compressible codes with two-equation turbulence models. It was found that the compressibility effect is significant when the leading edge is highly loaded, even at the low freestream Mach number. Both the parallelized incompressible and compressible codes adopting the PPCG algorithm can be efficient computational tools for multielement airfoil design.

Acknowledgments

This work was partially sponsored by the Korea Aerospace Research Institute and the Korea Research Foundation.

References

[1]Brune, G. W., and McMasters, J. H., "Computational Aerodynamics Applied to High-Lift System," *Applied Computational Aerodynamics*, edited by P. A. Henne, Vol. 125, Progress in Astronautics and Aeronautics, AIAA, Washington, DC, 1990, pp. 389–493.

[2]Rogers, S. E., Wiltberger, N. L., and Kwak, D., "Efficient Simulation of Incompressible Viscous Flow over Single and Multielement Airfoils," *Journal of Aircraft*, Vol. 30, No. 5, 1993, pp. 736–743.

[3]Rogers, S. E., and Kwak, D., "Upwind Differencing Scheme for the Time Accurate Incompressible Navier–Stokes Equations," *AIAA Journal*, Vol. 28, No. 2, 1990, pp. 253–262.

[4]Eyi, S., Lee, K. D., Rogers, S. E., and Kwak, D., "High-Lift Design Optimization Using the Navier–Stokes Equations," AIAA Paper 95-0477, Jan. 1995.

[5]Eyi, S., Chand, K., Lee, K. D., Rogers, S. E., and Kwak, D., "Multi-Element High-Lift Design Using the Navier–Stokes Equations," AIAA Paper 96-1943, June 1996.

[6]MPI-2: Extensions to the Message Passing Interface, Univ. of Tennessee, Knoxville, TN, 1996.

[7]Lee, B. S., and Lee, D. H., "Data Parallel Symmetric Gauss-Seidel Algorithm for Efficient Distributed Computing Using Massively Parallel Supercomputers," AIAA Paper 97-2138, June–July 1997.

[8]Shima, E., Egami, K., and Amano, K., "Navier–Stokes Computation of a High Lift System Using Spalart-Allmaras Turbulence Model," AIAA Paper 94-0162, Jan. 1994.

[9]Godin, P., Zingg, D. W., and Nelson, T. E., "High-Lift Aerodynamic Computations with One- and Two-Equation Turbulence Models," *AIAA Journal*, Vol. 35, No. 2, 1997, pp. 237–243.

[10]Woodruff, S. L., Morrison, J. H., and Hussaini, M. Y., "Evaluation of Several Turbulence Models in a Multiple-Element Airfoil Computation," AIAA Paper 98-0327, Jan. 1998.

[11]Kim, C. S., Kim, C., and Rho, O. H., "Computations of High-Lift Airfoil Flows Using Two-Equation Turbulence Models," AIAA Paper 99-0542, Jan. 1999.

[12]Wilcox, D. C., "Turbulence Modeling for CFD," DCW Industries, La Cañada, CA, 1993, pp. 73–170.

[13]Menter, F. R., "Two-Equation Eddy-Viscosity Turbulence Models for Engineering Applications," *AIAA Journal*, Vol. 32, No. 8, 1994, pp. 1598–1605.

[14]Wilcox, D. C., "Simulation of Transition with a Two-Equation Turbulence Model," *AIAA Journal*, Vol. 32, No. 2, 1994, pp. 247–255.

[15]Menter, F. R., "Influence of Freestream Values on the k–ω Turbulence Model Predictions," *AIAA Journal*, Vol. 30, No. 6, 1992, 1651–1659.

[16]Menter, F. R., and Rumsey, L. C., "Assessment of Two-Equation Turbulence Models for Transonic Flows," AIAA Paper 94-2343, June 1994.

[17]Roe, P. L., "Approximate Riemann Solvers, Parameter Vectors and Difference Schemes," *Journal of Computational Physics*, Vol. 43, 1981, pp. 357–372.

[18]Hwang, S. W., "Numerical Analysis of Unsteady Supersonic Flow over Double Cavity," Ph.D. Dissertation, Seoul National Univ., Seoul, Republic of Korea, 1996.

[19]Yoon, S., and Kwak, D., "Three-Dimensional Incompressible Navier–Stokes Solver Using Lower-Upper Symmetric-Gauss-Seidel Algorithm," *AIAA Journal*, Vol. 29, No. 6, 1991, pp. 874, 875.

[20]Steger, J. L., Doughty, F. C., and Beneck, J. A., "A Chimera Grid Scheme," *Advances in Grid Generation*, edited by K. N. Ghia, FED, Vol. 5, American Society of Mechanical Engineers, New York, 1983, pp. 59–69.

[21]Cook, P. H., McDonald, M. A., and Firmin, M. C. P., "Aerofoil RAE 2822—Pressure Distributions, and Boundary Layer and Wake Measurements," AR 138, AGARD, May 1979, pp. A6-1–A6-77.

[22]Coles, D., and Wadcock, A. J., "Flying-Hot-Wire Study of Flow Past an NACA 4412 Airfoil at Maximum Lift," *AIAA Journal*, Vol. 17, No. 4, 1979, pp. 321–329.

[23]Berg, B. v. d., "Boundary Layer Measurements On a Two-Dimensional Wing With Flap," National Aerospace Lab., TR 79009 U, Amsterdam, Jan. 1997.

[24]Braden, J. A., Whipkey, R. R., Jones, G. S., and Lilley, D. E., "Experimental Study of the Separating Confluent Boundary-Layer," NASA CR 3655, 1981.

R. M. C. So
Associate Editor